Pergamon

Int. J. Heat Mass Transfer. Vol. 37, Suppl. 1, pp. 191–205, 1994

0017-9310/94 $6.00 + 0.00

0017-9310(93)E0067-Q

Relating mechanics, blood flow and mass transport in the cardiac muscle

DANIEL ZINEMANAS, RAFAEL BEYAR and SAMUEL SIDEMAN

Heart System Research Center, The Julius Silver Institute, Department of Biomedical Engineering, Technion-Israel Institute of Technology, Haifa 32000, Israel

Abstract—Myocardial mechanics, perfusion and across-capillary mass transport are functionally related. The effects of these interacting phenomena on the performance of the left ventricle (LV) are investigated here. The effect of fluid balance on the diastolic and systolic intramyocardial pressures (*IMP*) and the interstitial and myocardial volumes as well as the global ventricular mechanics are of particular interest. The LV is approximated by a cylindrical geometry, containing blood vessels imbedded in the interstitial fluid and a fibrous matrix with active and passive elements. The coronary circulation is described by pressure dependent resistance–capacitance analog elements. Fluid and mass transport are calculated assuming an ideal semipermeable capillary wall and the lymphatic drainage depends linearly on the *IMP*. Changes in lymphatic flow are used to simulate edema formation, and its effects on myocardial mechanics and coronary flow. The empty beating and isovolumic contracting hearts are studied under constant coronary perfusion pressures. The model successfully predicts the corresponding changes of the coronary flow, the *IMP*, the LV pressure and the ventricular compliance. The simulated effects of a transient contractile dysfunction on the dynamics of fluid transport and coronary flow are in agreement with experimental data.

INTRODUCTION

MUSCLE mechanics, blood flow and intramural across-capillary fluid and mass transport are important interacting phenomena affecting the LV performance. As is well known, the vascular pressure is closely related to the *IMP* [1]; muscle mechanics play a dominant role in flow dynamics [2] and the coronary pressure has important effects on myocardial mechanics [3, 4]. Past theoretical investigations have considered the effects of LV mechanics on the myocardial flow [5–7], but do not include the effects of fluid and mass transport on the myocardial bed, and therefore cannot adequately predict the inverse effects of the coronary flow and perfusion pressure on the *IMP* and LV mechanics. Thus, for example, the diastolic *IMP* and the LV wall volume values are usually estimated input data in the LV mechanical models while, in fact, they depend on the coronary perfusion pressure and the fluid transport conditions. Similarly, coronary flow models depend on the *IMP* dynamics, which in turn depends on the muscle mechanics; fluid and mass transport models require capillary and *IMP* data which depend on LV mechanics and the coronary flow.

Accounting for the fluid transport and mass balance within the myocardium allows the effect of coronary flow on the *IMP* and LV mechanics to be evaluated. McCulloch *et al.* [4], for example, have studied the effect of coronary perfusion on the passive LV mechanics and suggest that fluid transport needs be accounted for, since small intravascular blood volume changes that may occur cannot explain the large observed changes in LV compliance. Kresh [2] suggests that the myocardium should be considered as a composite material of connective tissue, contractile elements, vessels, all interposed by an interstitial gel-like matrix.

The major goal of this paper is to extend our previous studies and develop an LV model that takes into account, simultaneously and interactively, the mechanics, the coronary blood flow and the fluid and mass transport phenomena. Particular attention is given here to the interaction between the calculated *IMP* in relation to the LV mechanics and coronary flow. The main advantage of this integrated model is its ability to relate the global LV performance (mechanics, coronary flow and fluid and mass transport) to the active myocardial properties and its structure at given loading conditions. The model predicts the *IMP* as a function of the mechanical flow and fluid and mass transport conditions and describes the associated multidirectional interactions. In addition, the model elucidates the pathophysiological mechanisms associated with disturbances in myocardial fluid balance such as in myocardial edema.

BASIC RELATIONSHIPS

The physiological model

As shown schematically in Fig. 1, the myocardium is a complex multi-component structure composed primarily of muscle fibers, which show a well defined spatial organization [8], and connective tissue, mainly collagen fibers, which connect between the muscle fibers. This complex matrix contains the coronary vessels, the interstitial fluid which fills the extravascular and extracellular space, and the lymphatic drainage into the venous system. The capillary walls are permeable to the transport of fluid and metab-

NOMENCLATURE

A	blood vessel cross sectional area
B	constant
C	blood vessel capacitance
c	solute concentration
D	constant
E	constant
F	volumetric flow
h	cardiac muscle thickness
IMP	intramyocardial pressure
J	mass flux
$k_{0,1,2,3,4}$	constants
K_c, K_r	constants
l_i	constant
L_p	capillary wall hydraulic conductivity
LVP	LV cavity pressure
n	normal unit vector
P	pressure
P_{per}	permeability coefficient
Q	blood volumetric flow
R	blood vessel resistance
R_G	gas constant
R_{in}	LV cavity inner radius
S	surface area
SL	sarcomere length
SL_0	minimum sarcomere length
SLP_0	passive unstrained sarcomere length
$t, \bar{T}$	time
T	Temperature
T_1	peak activation time
T_2	total activation time
V	volume.

Greek symbols

α	sarcomere orientation angle
β	rate of strain ratio
λ	stretch ratio
ν	reflection coefficient
Π	osmotic pressure
σ	stress tensor
σ_0	maximal muscle stress.

Subscripts

a	active
blood	blood
c	collagen
f	sarcomere fiber
fib	fiber
int	interstitial
lymph	lymphatic
LV	left ventricle
max	maximal
p	passive
r	radial direction
s	solute
tr	transmural
w	water
wall	LV wall
z	axial direction
0	reference state
θ	circumferential direction.

Superscripts

0	reference state.

olites. This mass transport is not only necessary for sustaining the muscle activity but at the same time it functionally relates between the muscle mechanics, the coronary flow and the fluid and mass transport. Moreover, the lymphatic outflow and macromolecular transport play an important role in the interstitial fluid and tissue volume control.

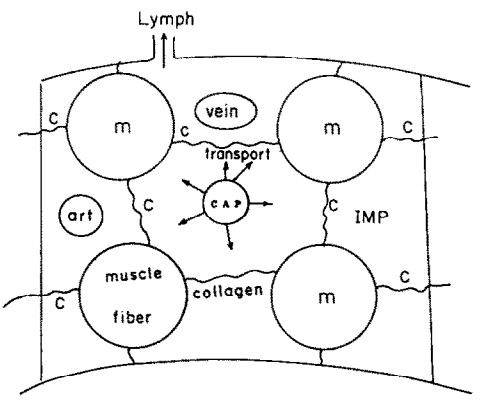

FIG. 1. Schematic description of the myocardial structure and components.

Muscle mechanics

Neglecting body forces and inertial effects, the myocardial stress field can be estimated by solving the force balance in the LV wall given by:

$$\nabla \cdot \boldsymbol{\sigma} = 0 \tag{1}$$

where $\boldsymbol{\sigma}$ represents the stress tensor. Since the myocardium is a complex structure of active (muscle fibers) and passive (collagen fibers) elements imbedded in the interstitial fluid, this tensor may be expressed by [9]

$$\boldsymbol{\sigma} = -P\mathbf{I} + \boldsymbol{\sigma}_a + \boldsymbol{\sigma}_p \tag{2}$$

where P denotes the interstitial fluid pressure, i.e. the IMP; $\mathbf{I}$ is the unit tensor and the subscripts a and p denote the active and passive stress components, respectively.

Equation (1) is complemented by the boundary con-

ditions denoting the normal force balance at the inner endocardial surface,

$$LVP = P-(\sigma_a+\sigma_p):\mathbf{nn} \tag{3}$$

and at the epicardial surface

$$0 = P-(\sigma_a+\sigma_p):\mathbf{nn} \tag{4}$$

where $\mathbf{n}$ is a unit outward vector normal to the endocardial and epicardial surfaces and LVP denotes the LV cavity pressure.

Although equation (1) has a simple form, it is highly complex due to the irregular myocardial boundaries and structure and the non linearity of the material constitutive laws. In order to solve for the three principal stresses and the IMP, equation (1) is usually supplemented by the incompressibility condition [9–13] and a given initial end-diastolic IMP value. This incompressibility condition implies that the LV wall volume is constant along the heart beat; it does not, however, provide the actual value of this volume or its dependence on the LV operating conditions.

To overcome this limitation, and consistent with the myocardial structure, the total LV wall volume is expressed here as the sum of the volumes of the myocardial components, i.e.

$$V_{wall} = V_{blood}+V_{int}+V_{fib} \tag{5}$$

where the blood volume, V_{blood}, and the interstitial volume, V_{int}, each represents about 15% of the total LV wall volume [14] and the fiber volume, V_{fib}, occupies 70% of the total normal LV wall volume. Obviously, the blood and interstitial volumes vary according to the mechanical, blood flow and fluid and mass transport conditions.

Blood flow

Myocardial flow models are usually electrical analogs which describe the response of the myocardial circulation to the mechanical parameters. Each level or section of the circulation is described by a resistive and a capacitive element or similar electric elements. The values of these resistances and capacitances are not well known and they vary considerably with the transmural pressure difference, P_{tr}, defined as the difference between the vascular pressure and the IMP. Clearly, both the blood flow and blood volume depend on the vascular to extravascular pressure difference.

Neglecting vessel length variations and assuming Poiseuille's law to apply through the coronary vascular bed, the resistance, R, in each section is inversely proportional to the (squared) cross section area of the vessel, i.e.

$$R = K_r\frac{1}{A^2}. \tag{6}$$

The capacitance, C, per unit length is defined as the change in cross sectional area with the change in the transmural pressure difference [15], i.e.

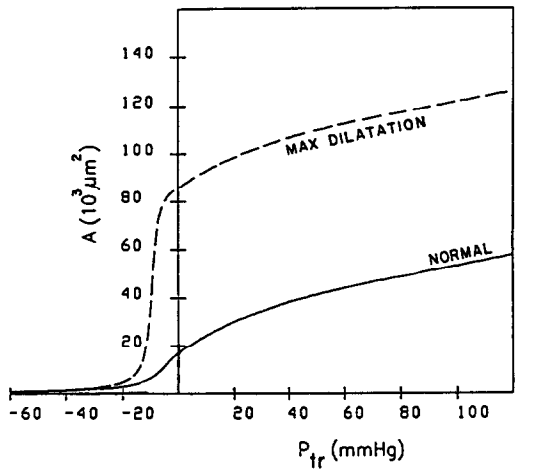

FIG. 2. The relationship between the vessel cross sectional area A and the transmural pressure difference, P_{tr} (reproduced from ref. [16], with permission).

$$C = K_c\frac{dA}{dP_{tr}} \tag{7}$$

where K_r and K_c are constants, set to fit the reported experimental resistance and capacitance values in the various types of vessels. The relationship between the vessel cross section area, A, and the transmural pressure difference is given in Fig. 2 [16].

Although flow predictions obtained with some refined models [5–7, 17] agree very well with experimental findings, the main limitation of these models is that they depend on given input values of the IMP, the LVP or the extravascular forces, which may vary in different physiological situations and can be, as is the IMP, difficult to measure.

Mass transport

For a simple system of a semipermeable membrane of the Kedem–Katchalsky [18] type that separates two fluid media which contain dilute solutions of various molecules, the fluid flux, J_w, essentially water, across the membrane is given by:

$$J_w = L_p(\Delta P-v\Delta\pi) \tag{8}$$

where L_p and v denotes the hydraulic conductivity and the reflection coefficients, respectively. $\Delta\pi$ is the interstitial to capillary osmotic pressure difference and $\Delta P = P_{cap}-IMP$, denotes the difference between the capillary pressure, P_{cap}, and the IMP. Equation (8) demonstrates clearly the direct dependence of the fluid transport rate on the blood flow and muscle mechanics since the capillary pressure and the IMP are both interactively determined by these two phenomena. For an ideal dilute solution the osmotic pressure difference is given by

$$\Delta\pi = R_G T\Delta c \tag{9}$$

where R_G denotes the gas constant, T is the absolute

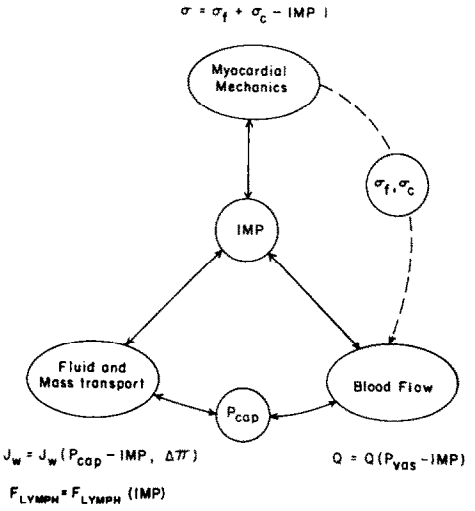

FIG. 3. Schematic description of the interactions between the LV mechanics, the coronary flow, and fluid and mass transport.

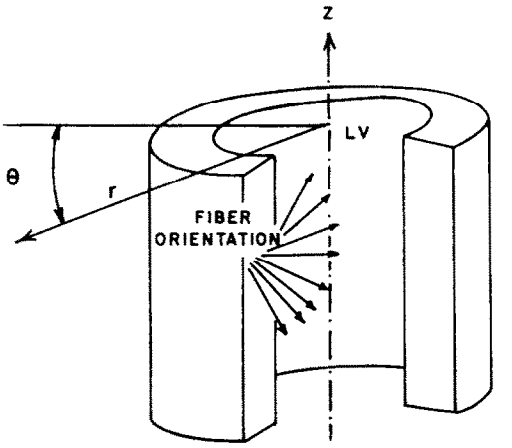

FIG. 4. Geometrical configuration and reference coordinates of a cylindrical LV wall.

temperature and Δc is the solute concentration difference.

The solute flux, J_s, is given by the sum of the convective and diffusive terms

$$J_s = J_w(1-v)\frac{(c_{cap}+c_{int})}{2} + P_{per}(c_{cap}-c_{int}) \quad (10)$$

where P_{per} is the membrane permeability coefficient, and the subscripts cap and int denote the capillary and the interstitium, respectively.

The mass conservation principle for the total interstitial volume, is given by:

$$\frac{\partial V_{int}}{\partial t} = S_{cap}J_w - F_{lymph} \quad (11)$$

where F_{lymph} is the lymphatic flow. Similarly, the total solute mass balance is given by:

$$V_{int}\frac{\partial c_{int}}{\partial t} = S_{cap}J_s - F_{lymph}c_{int} - c_{int}\frac{\partial V_{int}}{\partial t} \quad (12)$$

where S_{cap} is the capillary wall area. Since albumin, the largest macromolecule in the plasma, is dominant in determining the osmotic pressure difference, we consider only this species in this model. Note that the *IMP* is the driving force for the lymphatic flow. Moreover, under steady state conditions, the net transcapillary fluid flow equals the lymphatic outflow. Thus, equations (11) and (12) determine the interstitial fluid content and provide an additional relationship between the mechanical and flow parameters which also needs to be observed.

THE INTEGRATED MODEL

The basic links between muscle mechanics, coronary flow and the fluid and mass transport, are schematically represented in Fig. 3. Basically, these interactions indicate that the mechanics affects the blood flow and the fluid and mass transport through the *IMP* and fiber stresses, but at the same time the blood flow and the fluid and mass transport affect the mechanics by changes in the myocardial blood and interstitial fluid content. It is, therefore, evident that these three phenomena cannot be simply decoupled, but need to be considered integratively as a whole if the LV performance is to be uniquely determined. Clearly, any change in one of these three phenomena will eventually affect the other two and consequently the whole LV function. Even in the case that the muscle and collagen stresses are dominant in determining the flow behavior, the flow still affects the *IMP* through the capillary pressure and the fluid and mass transport, which indirectly affect the LV mechanics.

The current model is based on a cylindrical geometrical approximation (Fig. 4) [10], with the LV wall composed of a network of muscle fibers with a changing fiber angle distribution across the wall [8], and a collagen matrix imbedded in the interstitial fluid. The collagen fibers lie in a 3-dimensional matrix, parallel and perpendicular to the muscle fibers on the cylindrical surfaces and as well as in the radial direction. The blood vessels inside this configuration are primarily affected by the *IMP*.

The combined effect of the interactions between myocardial mechanics, blood perfusion and mass exchange between the blood vessels in the myocardial tissue is obtained here by the simultaneous and interactive solution of the basic equations that describe these phenomena and their relationships. Only average values of the transmural stresses, strains and other variables are used here.

Mechanical model

Using the constitutive equation for the myocardial stresses, equation (2), and averaging these stresses across the LV wall (thin wall approximation), the myocardial force balances are given by:

$$LVP = \frac{h}{R_{in}}(\sigma_{\theta f}+\sigma_{\theta c}-IMP);\ \theta\text{-direction} \quad (13)$$

$$LVP = \frac{2h}{R_{in}}\left(1+\frac{h}{2R_{in}}\right)(\sigma_{zf}+\sigma_{zc}-IMP);\ z\text{-direction}. \quad (14)$$

Here h is the wall thickness, R_{in} is the radius of the inner cylinder, which in terms of the midwall radius, $\bar{R}$, is given by $R_{in} = \bar{R}-h/2$; $\sigma_{\theta f}$ and σ_{zf} denote the average muscle stress in θ and z directions, respectively; $\sigma_{\theta c}$ and σ_{zc} are the corresponding collagen average θ and z stress.

The relationship accounting for the radial myocardial stresses is derived from the boundary conditions, equations (3) and (4), yielding the following radial force balance

$$\frac{LVP}{2} = IMP-\sigma_{rc} \quad (15)$$

where σ_{rc} is the average radial stress.

Muscle fiber stresses are composed of an active and a passive component. A non-symmetric activation waveform [19] is approximated by a square sinus function. The active part of the muscle fiber stresses, σ_f, is then given by:

$$\sigma_f = \begin{cases} \sigma_{f,max}\cdot\sin^2\left[\dfrac{\pi t}{2T_1}\right]; 0 < t < T_1 \\ \sigma_{f,max}\cdot\sin^2\left[\dfrac{\pi(t-T_1)}{2(T_2-T_1)}\right]; T_1 < t < T_2 \end{cases} \quad (16)$$

where T_2 and T_1 denote the total and peak activation times, respectively. The maximum normalized isometric stress, $\sigma_{f,max}$, is given by [20]:

$$\sigma_{f,max} = \begin{cases} \dfrac{(SL-SL_0)\sigma_0}{0.55}; 1.65 < SL < 2.2\mu \\ \sigma_0; 2.2 < SL < 2.4\mu \\ \sigma_0-\dfrac{(SL-2.4)\sigma_0}{0.55}; SL > 2.4\mu \end{cases} \quad (17)$$

where σ_0 is the maximum stress and SL_0 denotes the minimum sarcomere length required for active stress development.

The passive muscle fiber stresses are given by [21]:

$$\sigma_{fp} = \begin{cases} D(e^{E(\lambda-1)}-1) & \lambda > 1 \\ -B(\lambda-1) & \lambda < 1 \end{cases} \quad (18)$$

where D and E are material constants and the muscle stretch ratio, λ, is given by the ratio of the sarcomere length, SL, to the sarcomere length at the passive unstrained state, SLP_0,

$$\lambda = \frac{SL}{SLP_0}. \quad (19)$$

The stress to rate of strain ratio β [22] is approximated by [11]:

$$\beta = \frac{\beta_{max}}{\sigma_f}(\sigma_0-\sigma_f) \quad (20)$$

where β_{max} is the maximal stretch rate. The collagen fiber stresses are described by the nonlinear relationship [13]

$$\sigma_c = D_c[e^{E_c(\lambda_c-1)}-1]. \quad (21)$$

The wall-averaged stress components of the muscle fibers in the θ and z directions are calculated from the individual stresses and the fiber orientation distributions

$$\sigma_{\theta f} = \frac{1}{2\alpha_0}\int_{-\alpha_0}^{\alpha_0}\sigma_f(\alpha)\cos^2\alpha\,d\alpha \quad (22)$$

and

$$\sigma_{zf} = \frac{1}{2\alpha_0}\int_{-\alpha_0}^{\alpha_0}\sigma_f(\alpha)\sin^2\alpha\,d\alpha \quad (23)$$

where α_0 denote the limits of the muscle fiber orientation. The fiber orientation in the unstressed state is assumed to vary linearly from the endocardium to the epicardium in the range -60 to $+60°$. The expressions for the collagen stresses in the muscle fiber direction are the same as equations (22) and (23). For the collagen fibers in the same plane but perpendicular to the muscle fibers, the expressions for the stresses are similar but the *sine* and *cosine* are interchanged.

The instantaneous wall volume is related to the wall deformations through the expression

$$V_{wall}(t) = \lambda_r\lambda_\theta\lambda_z V^0_{wall} \quad (24)$$

where V^0_{wall} denotes the wall volume at the *unstressed reference state*, which is defined as the state where the LVP, the IMP, the P_{vas} and the osmotic gradient, $\Delta\pi$, are all zero.

The requirement that the cavity volume remains constant during the contracting and relaxing isovolumic stages, expressed as the ratio between the isovolumic and the reference state cavity volumes, is given by:

$$\lambda_z\frac{\left[\lambda_\theta-\dfrac{h_0}{2\bar{R}_0}\lambda_r\right]^2}{\left[1-\dfrac{h_0}{2\bar{R}_0}\right]^2} = \frac{V_{LV}(LVP^0)}{V_{LV}(LVP^0=0)} \quad (25)$$

where LVP^0 is the pressure at the beginning of the isovolumic stage. h_0, $\bar{R}_0$ and V^0_{LV} denote wall thickness, midwall radius and LV volume in the unstressed reference state, respectively.

Finally, geometric compatibility requires that the deformation of the muscle and collagen fibers should match the overall myocardial deformation. This is mathematically expressed by:

$$\lambda_f = \sqrt{(\lambda_\theta^2\cos^2\alpha+\lambda_z^2\sin^2\alpha)}. \quad (26)$$

A similar expression holds for collagen fibers run-

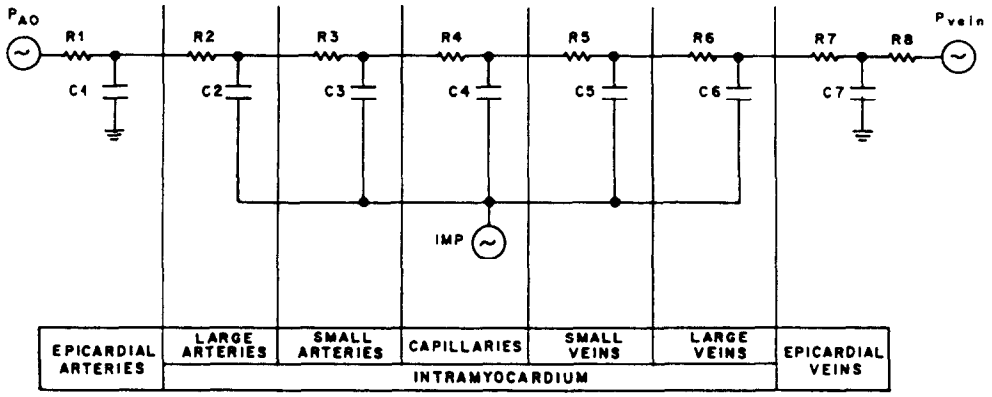

FIG. 5. Electrical analog of the myocardial circulation.

ning parallel to the muscle fibers. For collagen fibers perpendicular to muscle fibers, in the (θ, z) plane, the stretch ratio is given by equation (26), but with interchanged *sine* and *cosine*. The stretch of the collagen in the r direction equals the stretch of the wall, λ_r.

The rate of strain of the muscle fiber is determined from the time derivative of equation (26), i.e.

$$\beta = -\frac{d\lambda_f}{dt} = -\frac{1}{\lambda_\theta}\left(\lambda_\theta \cos^2\alpha \frac{d\lambda_\theta}{dt} + \lambda_z \sin^2\alpha \frac{d\lambda_z}{dt}\right). \quad (27)$$

The instantaneous orientation α' of a given fiber is related to its initial orientation α and the overall myocardial deformation by:

$$\alpha' = \arctan\left[\tan(\alpha)\frac{\lambda_z}{\lambda_\theta}\right]. \quad (28)$$

Flow model

Pressure and flows in the vasculature are calculated by means of a blood vessel transmural pressure dependent resistance–capacitance electrical analog model (Fig. 5). The analysis follows the work of Beyar *et al.* [16], but for simplicity it considers the myocardium as one compartment, thus averaging transmural flow heterogeneities, and includes an additional capillary compartment which is necessary to evaluate the fluid and macromolecular transport across the capillary wall. Importantly, changes in vascular volumes that occur throughout the cycle or due to different working conditions are also accounted for in the general solution of the integrated model.

The resistance R and the capacitance C corresponding to each vessel type in Fig. 5 are functions of the vessel transmural pressure difference, $(P_{vas} - IMP)$, through their dependence on the vessel's cross sectional area (equations (6) and (7)). The cross sectional area depicted in Fig. 2 is approximated by [16, 23]

$$A = k_0 + k_1 P_{tr} + k_2 P_{tr}^2 + k_3 P_{tr}^3 + k_4 P_{tr}^4; P_{tr} > 0 \quad (29)$$

$$A = A_0\left[1 + \frac{2}{\pi}\operatorname{atan}[(P_{tr} - P_0)/E]\right]; P_{tr} < 0 \quad (30)$$

where k_i, P_0, E, and A_0 are constants. As stated above the values of K_r and K_c in equations (5) and (6) are determined by assuming a mean normal flow of 1 ml s^{-1}-100 gr^{-1} LV and a distribution of resistance corresponding to the experimental findings of Chilian *et al.* [24], i.e. 25% pressure drop in the large arteries, 68% in the microvessels and 7% in the veins. Following Kresh *et al.* [17], 20% of the total pressure drop is assigned to the capillary part of the microvessels. Mean values of the capacitances are assumed, following Spaan [15]: 0.0022 ml $mmHg^{-1}$-100 gr^{-1} LV in the large arteries, 0.013 ml $mmHg^{-1}$-100 gr^{-1} LV in the small arteries, 0.035 ml $mmHg^{-1}$-100 gr^{-1} LV in the capillaries, 0.043 ml $mmHg^{-1}$-100 gr^{-1} LV in the small veins and 0.045 ml $mmHg^{-1}$-100 gr^{-1} LV in the large veins.

The differential equation which must be solved at each node i of the electrical analog is given by

$$\frac{dP_{vas}^i}{dt} = \frac{P_{vas}^{i-1} - P_{vas}^i}{R^i C^i} - \frac{P_{vas}^i - P_{vas}^{i+1}}{R^{i+1} C^i} + \frac{dP_{out}}{dt} \quad (31)$$

where P_{out} denotes the external pressure, i.e. zero for the epicardial arteries and veins and equal to the IMP for the intramural vessels.

The total blood volume can be calculated using the expression

$$V_{blood} = \sum_i l_i A_i \quad (32)$$

where A_i are the cross sectional area of vessels of the i class and l_i are constants chosen so that the distribution of blood volumes agrees with the experimental value, i.e. the reference total blood volume is assumed to be 15 ml 100 gr^{-1}-LV at the perfusion pressure of 100 mmHg. Of the total 15 ml, 3 ml are assigned to the large vessels, 7 ml to the medium size vessels and 5 ml to the capillary bed. Given the initial

blood volume, the total blood volume changes are described by the total blood mass balance given by:

$$\frac{dV_{blood}}{dt} = Q_{blood_{in}} - Q_{blood_{out}} \quad (33)$$

where Q_{blood} is the coronary volumetric flow and the subscripts in and out denote the inflow and outflow, respectively.

Fluid transport

Since the time scale for fluid and macromolecular transport is generally much larger than one heartbeat, the steady state solution of equations (11) and (12) can be used in the numerical procedure for the arrested and the steady state beating heart. The steady state solution of equation (11) is given by:

$$L_p S_{cap}\left[\bar{P}_{cap} - \overline{IMP} - v\Delta\pi(c)\right] = F_{lymph}(IMP_d) \quad (34)$$

where $\bar{P}_{cap}$ denotes the time and space average capillary pressure during one beat and $\overline{IMP}$ is the time average of the IMP. The total heart lymphatic flow, F_{lymph}, is given by an empirical linear function of the diastolic IMP [1]:

$$F_{lymph} = F^0_{lymph}[1 + 0.12(IMP_d - 15)] \quad (35)$$

where the lymphatic flow, $F^0_{lymph} = 7$ [ml h^{-1}] at a diastolic $IMP_d = 15$ mmHg. This linear relationship indicates that there is an increase of 12% in the lymphatic flow for each mmHg increase of the diastolic IMP. Although equations (34) and (35) are useful for steady state calculations, analysis of transient situations requires a rigorous solution of the mass balances, equations (11) and (12). Note that equation (35) allows us to perform the calculations in the absence of a model for the myocardial lymphatic flow.

The steady state solution of equation (12), which gives the ratio of the interstitial albumin concentration to the (known) capillary concentration and allows us to calculate the osmotic contribution in the arrested heart and steady state beating heart conditions, is given by [25]:

$$\frac{c_{lymph}}{c_{cap}} = \frac{\left[\frac{(1-v)}{2} + \frac{P_{per}S_{cap}}{V_{lymph}}\right]}{\left[\frac{(1+v)}{2} + \frac{P_{per}S_{cap}}{F_{lymph}}\right]}. \quad (36)$$

The values of the parameters involved in the model (mechanical, flow, fluid and macromolecular transport) are given in Table 1.

Analysis of the empty beating and the isovolumic contracting hearts

The LV model presented here can be used for any loading conditions by simply connecting it to an appropriate systemic circulatory model [11, 26]. Here, we focus our attention on two important experimental conditions: (1) the empty beating heart ($LVP = 0$), and (2) the isovolumic contracting heart. Both conditions are studied under constant coronary perfusion pressures; this simplifies the theoretical analysis and allows comparison with very well defined and controlled experimental conditions [2, 27–29]. These situations are particularly interesting since they represent two extreme cases of the coupling between muscle mechanics and flow; the former corresponds to a zero afterload situation, where the effect of cavity pressure on the circulation is zero and muscle deformation is maximal; the latter corresponds to an infinite afterload where the effect of the cavity pressure on the flow is maximal and muscle deformations are small. To model the empty beating heart, we impose $LVP = 0$ in the force balances, equations (13)–(15), and discard the isovolumic constrain, equation (25).

The results can be compared to the experimental data of Krams *et al.* [27, 28], who studied these two cases experimentally. Kresh *et al.* [2, 29] have studied the effect of coronary perfusion pressure and contractile conditions on the coronary blood flow and the IMP in the empty beating and arrested hearts.

Numerical procedure

The numerical algorithm addresses, interactively, the force balances, equations (13)–(15), the flow equations, equation (31), and the fluid and mass transport balances, equations (11) and (12), given the geo-

Table 1. Values of the parameters used in the model

(A) Mechanics

σ_0	900, 1300	[gr cm^{-2}]	(700, 1000 [mmHg])
D, D_c	6	[gr cm^{-2}]	
E, E_c	10	[gr cm^{-2}]	
B	10		
SL_0	1.65	[μm]	
β_{max}	3	[s^{-1}]	
α	60°		
R_0	2.5	[cm]	
h_0	1.2	[cm]	

(B) Flow

	k_r 10^{-10} mmHg s^{-1} 100 gr^{-1} LV	k_c 10^5 cm
	cm	100 gr LV
Large arteries	28 000	0.01
Small arteries	42 000	0.01
Capillaries	7000	0.022
Small veins	230	0.03
Large veins	70	0.09

(C) Fluid transport

L_p	10^{-8}	[cm s^{-1} mmHg^{-1}]
v	0.87	
P_{er}	5×10^{-8}	[cm s^{-1}]
S_{cap}	1.35×10^5	[cm^2]
F^0_{lymph}	1.93×10^{-3}	[ml s^{-1}]

metrical and boundary conditions, equations (24) and (25) and using the related constitutive equations and the quantitative definitions of the various parameters involved.

Arrested heart. The steady flow, fluid and mass transport are first calculated by solving simultaneously, using an iterative method, the steady state flow and fluid and mass transport equations (i.e. equations (31) with the vascular and intramyocardial pressure time derivatives equal to zero), and the mass balances (equations (34) and (36)). The solution of this system yields the values of the *IMP* and the flow variables. Given the *IMP* value, the force balances (equations (13)–(15)) are solved, employing a Newton–Raphson method to obtain the total wall volume change and fiber deformations. Once the total wall volume is known and the total blood volume is evaluated from equation (32), the interstitial volume is found from equation (5) and the given volume of fibers.

Beating heart. The variables obtained in the arrested heart conditions are used as initial conditions for the subsequent beating heart calculations which are initiated by starting the muscle activation wave [14]. Steady state beating heart conditions are obtained by simultaneous solution of the quasi-steady force balances (equations (13)–(15)), the geometrical constrains for the wall (equation (24)), and the cavity (equation (25)) volumes, and the blood flow (equations (31)), throughout the cardiac cycle. This provides the wall deformation dynamics (λ_θ, λ_r, λ_z), the *IMP*, the *LVP* and the blood flow and pressures. The instantaneous total blood volume is updated by integrating equation (33), using a simple Newton method, and this value is used to update the total wall volume (equation (5)), during the cardiac cycle.

Since the time constants for fluid and mass transport, which range from seconds to hours [30], are larger than a single beat, the interstitial fluid volume is assumed constant during a single cardiac cycle, but is updated on a beat to beat basis. Thus, integration of equations (11) and (12) follows the interstitial volume and macromolecular concentration dynamics, and is performed in time increments equal to the cardiac cycle. The time dependent equation (5)

$$V_{\text{wall}}(t) = V_{\text{blood}}(t) + V_{\text{int}}(\bar{T}) + V_{\text{fib}} \qquad (37)$$

then substitutes the generally assumed myocardial incompressibility condition. Note that $\bar{T}$ denotes a beat to beat (or larger) time scale. The effects of blood volume changes during a heart beat or the interstitial fluid changes on larger time scales, can thus be evaluated. Blood flow and volume changes are calculated using the flow equations (31) and the total blood mass balance, equation (33), with the end-diastolic or initial blood volume calculated from equation (32).

The algorithm for calculating the steady state beating heart conditions is in fact the transient procedure to calculate the steady state solution starting from the arrested heart conditions. This transient algorithm may, however, be time consuming since the mass transients are longer than the flow transients. An alternative way to accelerate the numerical convergence from the arrested to the steady state solution is to use a pseudo-transient solution by imposing, at the end of each cardiac cycle, the steady state mass balances, equations (34) and (36), instead of solving the transient balances, equations (11) and (12). This approach allows us to estimate the changes in the end-diastolic *IMP* directly instead of calculating the *IMP* changes that follow from the interstitial volume dynamics at the end of each cardiac cycle. As expected, both procedures give the same steady state solution. However, the first procedure is essential to calculate transient responses, and the second pseudo-transient procedure is useful only to calculate steady state conditions.

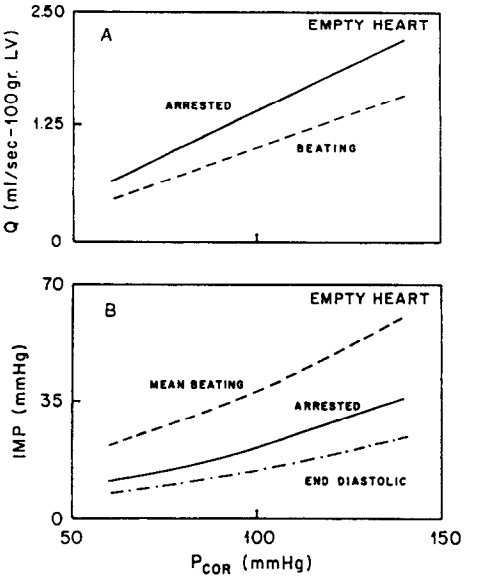

FIG. 6. Mean myocardial flow (A) and mean and end-diastolic *IMP* (B) vs coronary perfusion pressure in the arrested and the beating heart.

RESULTS

The mean coronary flow rate and the mean and end-diastolic *IMP*s are presented in Figs. 6(A) and (B) as functions of the coronary pressure, P_{cor}, in the empty ($LVP = 0$) arrested and beating hearts. The lymphatic flow has been assumed to follow equation (35) in both these situations, with equilibration of fluid transport at each pressure. As seen, the flow rate increases with the perfusion pressure and the flow rate as well as its slope is larger in the arrested than in the beating heart. Correspondingly, the *IMP* (Fig. 6(B)) increases with the perfusion pressure and is higher in the beating than in the arrested heart thus explaining the larger flow rates in the arrested heart. These results are consistent with the experimental data of Kresh *et al.* [29] and Baird *et al.* [31] for the empty beating heart. It is interesting to note to that the *IMP* in the

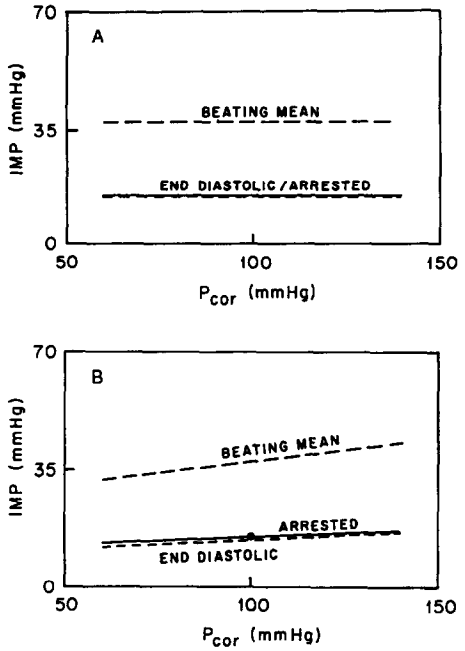

FIG. 7. Mean myocardial flow (A) and mean and end-diastolic *IMP* (B) vs coronary perfusion pressure in the arrested and the beating heart without accounting for fluid and mass transport effects.

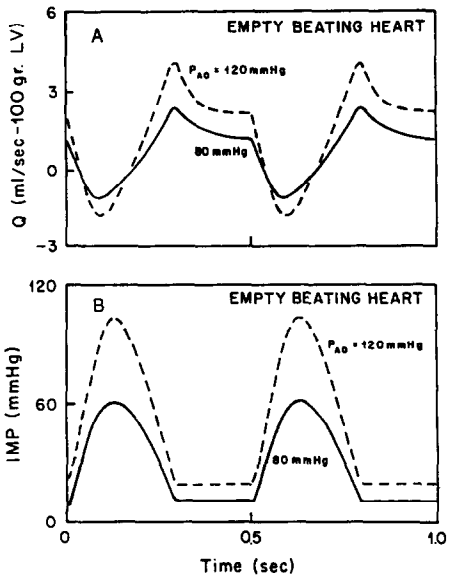

FIG. 8. Dynamics of the coronary flow (A) and the *IMP* (B) in the empty beating heart at different perfusion pressures. P_{cor} = 80 mmHg, P_{cor} = 120 mmHg.

arrested heart is higher than the IMP_d in the beating heart. This is due to the different fluid and blood content in the myocardial wall in these two cases, i.e. the interstitial and total wall volumes are larger in the arrested heart than in the beating heart due to the smaller mean *IMP* in the former case. The predicted end-diastolic IMP_d value of 15 mmHg at a perfusion pressure of 100 mmHg is in accordance with the reported experimental data of Laine and Granger [1].

For comparison, the above calculations were repeated for two additional cases: (1) no fluid transport and coronary effects, i.e. the vascular and interstitial volumes are constant, and (2) only coronary effects, i.e. changes in vascular volume due to changes in the perfusion pressure, are accounted for but the interstitial volume is constant. The results, depicted in Fig. 7(A), show that when fluid and mass transport as well as coronary effects are neglected the coronary pressure does not affect the LV mechanics since changes in the LV wall volume due to changes in vascular or interstitial volumes are not accounted for. Furthermore, the values of the arrested and end-diastolic *IMP*s are unknown and must be independently assumed. When the vascular volume changes with the change in the perfusion pressure are accounted for (Fig. 7(B)), the changes in the *IMP* with the perfusion pressure can be predicted. The results in Fig. 7 were obtained assuming that *IMP* = 15 mmHg at a perfusion pressure of 100 mmHg and that the combined interstitial and fiber volume is 85 ml 100 gr^{-1}-LV. The reference point is depicted in Fig. 7(B) by a dot. Note that the interstitial fluid volume which normally changes with the perfusion pressure, is kept constant in these particular calculations, and that the diastolic and systolic *IMP* dependence on the perfusion pressure is weaker than in the case where both coronary flow and mass transport effects are considered (Fig. 6(B)).

The correspondence of the flow rate in the epicardial arteries and the *IMP* at steady state conditions and at two different perfusion pressures is shown in Figs. 8(A) and (B). Consistent with Krams *et al.* [28] the oscillatory flow amplitude increases as the perfusion pressure increases.

The oscillatory flow amplitude (*OFA*) in the empty beating heart is plotted in Fig. 9 as a function of the perfusion pressure at two different maximum sarcomere stresses, σ_0 = 700 and 1000 mmHg, representing two different contractility states. Consistent with experimental data [2, 28], these results show an increase of the *OFA* with an increase of the perfusion

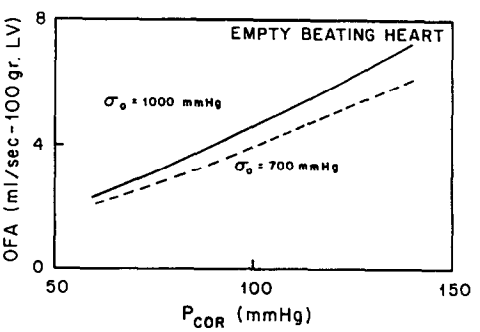

FIG. 9. Oscillatory flow amplitude (*OFA*) vs perfusion pressure at two different maximum sarcomere stresses, σ_0 = 700 and 1000 mmHg.

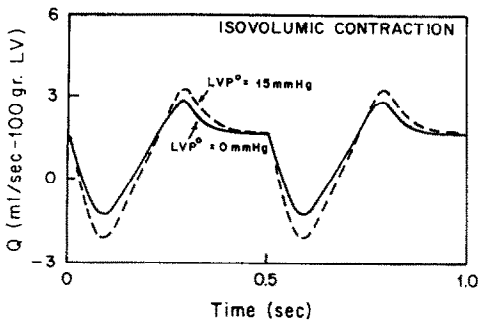

FIG. 10. Dynamics of the coronary flow in the isovolumic contracting heart at a perfusion pressure of 100 mmHg and at two different diastolic pressures. $LVP^0 = 0$ and 15 mmHg.

pressure and with increased contractility. The increase of the *OFA* with perfusion pressure may be explained by an increase in the amplitude of the *IMP* oscillation (Fig. 8(B)) but may also include a contribution from a change in the distribution of the intramyocardial resistances. The lower values of the *OFA* at reduced values of the maximal muscle stress reflect the lower values and oscillatory amplitude of the *IMP* at a lower contractility.

The flow waveforms in the isovolumic contracting heart are shown in Fig. 10 for a constant perfusion pressure of 100 mmHg at two different end-diastolic volumes, $LVP^0 = 0$ and 15 mmHg. It is noted that the flow waveforms in this case are qualitatively and quantitatively similar to those of the empty beating heart presented in Fig. 8(A), although the LV cavity pressure is entirely different. This fact can be explained by the similar *IMP* waveforms obtained in both cases despite the great difference in the ventricular load and deformation dynamics. Another feature of Fig. 10 is the change in *OFA* with the preload. By changing the preload, Krams *et al.* [28] show that the *OFA* is practically independent of the developed pressure (i.e. systolic minus diastolic *LVP*) in the isovolumic feline heart. However, Abel *et al.* [32], using canine hearts, show that increasing the peak *LVP* by controlling the afterload causes an increase in the *OFA*. The corresponding calculated *LVP* and *IMP* in an isovolumic contraction with $LVP^0 = 0$ are shown in Fig. 11. The

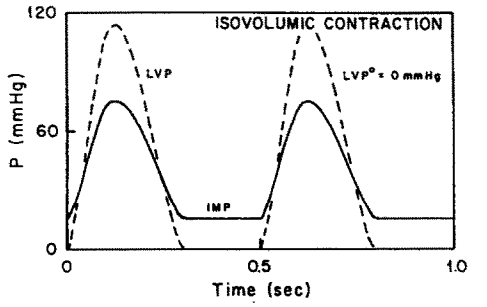

FIG. 11. Dynamics of the *IMP* and *LVP* in the isovolumic contracting heart at a diastolic $LVP^0 = 0$.

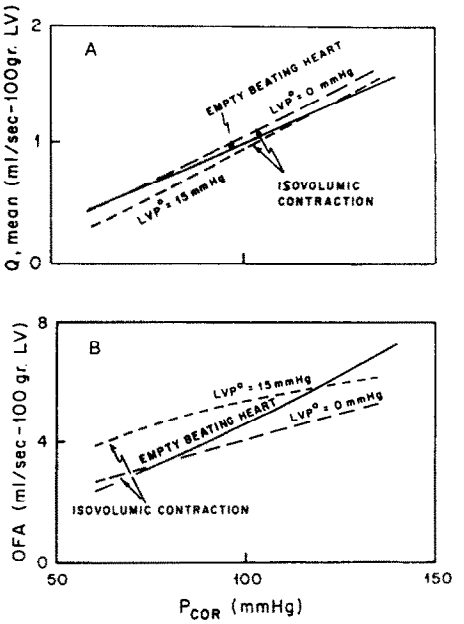

FIG. 12. Mean coronary flow (A) and oscillatory flow amplitude (*OFA*) (B) vs perfusion pressure in the empty beating and in the isovolumic contracting heart at two different preloads. $LVP^0 = 0$ and 15 mmHg.

calculated *LVP* waveform corresponds to the experimental findings of Krams *et al.* [28]. Note that while during diastole $LVP = 0$ the corresponding *IMP* is not zero.

A comparison between the isovolumic and the empty beating hearts in terms of the effects of the perfusion pressure and the diastolic cavity pressure on the mean coronary flow and the *OFA* is presented in Figs. 12(A) and (B). The mean coronary flow–pressure relationship is quite similar for the two cases (Fig. 12(A)), showing a small decrease in the mean flow with an increase in the preload and the corresponding increase in the peak systolic LV pressure which is consistent with the data of Abel *et al.* [32]. Reasonably similar *OFA* values in the two hearts are in agreement with the experimental data of Krams *et al.* [28], suggesting a small direct effect of the *LVP* on the *OFA*. As mentioned in connection with Fig. 10, the model predicts a slight increase of the *OFA* with increasing preload, which is larger than the results reported by Krams *et al.* [28]. Abel *et al.* [32], however, show that the *OFA* increases with the increase in peak systolic pressure.

All the results presented here correspond to the normal values of the vasculature tone without the autoregulatory mechanisms. Similar calculations for maximum vasodilation do not show a qualitative difference from the normal vascular tone without autoregulation. However at the different resistances and capacitances of the blood vessels under maximum vasodilation, the flow increases about 400% and the *OFA* increases by a factor of 2. The *IMP* dependence

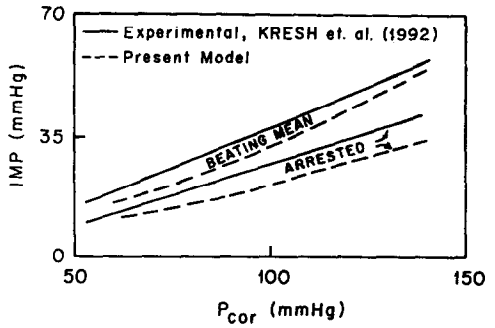

FIG. 13. Mean *IMP* vs coronary perfusion pressure in the arrested and the beating heart with maximal vasodilated state.

on the perfusion pressure for the vasodilated case is shown together with the experimental empty beating heart data of Kresh *et al.* [29] in Fig. 13.

The predicted *OFA* with maximal vasodilation is compared with the data of Krams *et al.* [28], and shown in Fig. 14. Considering the scatter of the data and that the fact that no parameter optimization was performed but the values (obtained mainly for dogs and not cats) reported in the literature were used this comparison is quite satisfactory.

Kresh [2] measured the *IMP* and the coronary flow in a vented (empty) beating isolated heart, which was perfused at a constant pressure by a Krebs–Henseleit solution. The heart was then transiently arrested by an infusion of pentobarbital. The experiment suggests that the time scale of the fluid transport and the washout of the pentobarbital, i.e. the mechanical effect, are of the same order of magnitude. The model results are compared in Fig. 15 with the experimental results. In simulating this experiment we have assumed that the heart muscle is a continuously stirred tank reactor (CSTR) so that the bolus of pentobarbital rapidly increases the 'reactor's' concentration up to a maximum value, followed by an exponential fall of the concentration. The effect of the pentobarbital on the sarcomere force, σ_0, is assumed to be inversely proportional to its concentration in the myocardium.

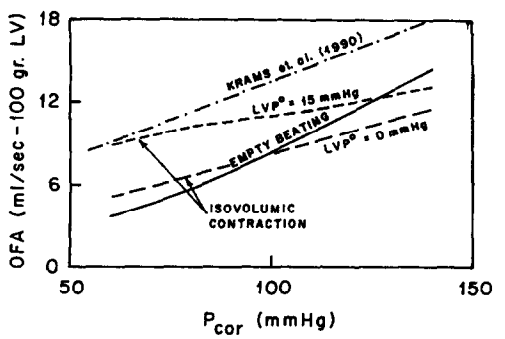

FIG. 14. Oscillatory flow amplitude (*OFA*) vs perfusion pressure in the empty beating and in the isovolumic contracting heart at two different preloads $LVP^0 = 0$ and 15 mmHg and maximal vasodilated state.

The sarcomere force is assumed to be zero at the maximum concentration. Once the effect of pentobarbital is over, the flow oscillations resume and the system returns to its previous steady state. Inspection of Fig. 15 shows that the analytical simulation closely follows the trends of the experimental data.

Myocardial edema is another example highlighting the importance of the fluid and mass transport in the integrated model in cases of myocardial pathology. An edematous state is simulated here by reducing the lymphatic flow (equation (35)). The trend of the results obtained by keeping all other parameters constant, but reducing the lymphatic flow to a third of its normal value, i.e. $F_{lymph} = 2.3$ ml h^{-1}, reduces the normal mean myocardial flow and increases the mean *IMP* and the *OFA*; these differences increase monotonically with the increase of the perfusion pressure. Quantitatively, a reduction of 12% in the mean flow and an increase of 15% in the *IMP* and 17% in the *OFA* are predicted for reduced lymphatic flow in the empty beating heart, at a perfusion pressure of 100 mmHg. The total wall volume increases by 4% and the interstitial volume by 37%. The blockage of the lymphatic flow increases the mean *IMP* due to the increase of myocardial fluid content and thus induces the decrease of the mean myocardial flow. Obviously, keeping all but the lymphatic parameters constant may not be realistic since, for example, changes in flow may cause changes in sarcomere activity, and the capillary wall hydraulic conductivity may also change, thus enhancing the edema phenomena. However, the general trend of decreased flow and increased *IMP* will most likely prevail. Evidently, a decrease in the myocardial blood flow and an increase in the interstitial fluid will reduce the metabolic supply to the muscle, and consequently will directly affect the sarcomere contractile activity.

The effect of the perfusion pressure on LV compliance, dV/dP, for the isovolumic contracting heart is presented in Table 2. A decrease in diastolic ventricular compliance is predicted for increasing perfusion pressure associated with an increase in the myocardial fluid content and total volume. The values shown in Table 2 agree very well with the experimental data of Fukui *et al.* [3] showing C_{ED} values of 1.25 and 0.66 ml $mmHg^{-1}$ at perfusion pressures of 70 and 150 mmHg, respectively.

The total blood volume changes during a single heart beat are calculated by the model to be of order of 0.5 ml 100 gr^{-1}-LV, which corresponds to $\approx 0.5\%$ of the total wall volume or $\approx 3\%$ of the total blood volume. The corresponding effects on the overall LV variables, such as the blood flow rate or the *OFA*, are found to be of the same order of magnitude, i.e. $\approx 0.5\%$. These hardly differ from the case when the blood volume is assumed constant throughout the cardiac cycle. Total blood volume changes may be more important in transient cases or during changing working conditions, and in larger time scales than the one cardiac cycle.

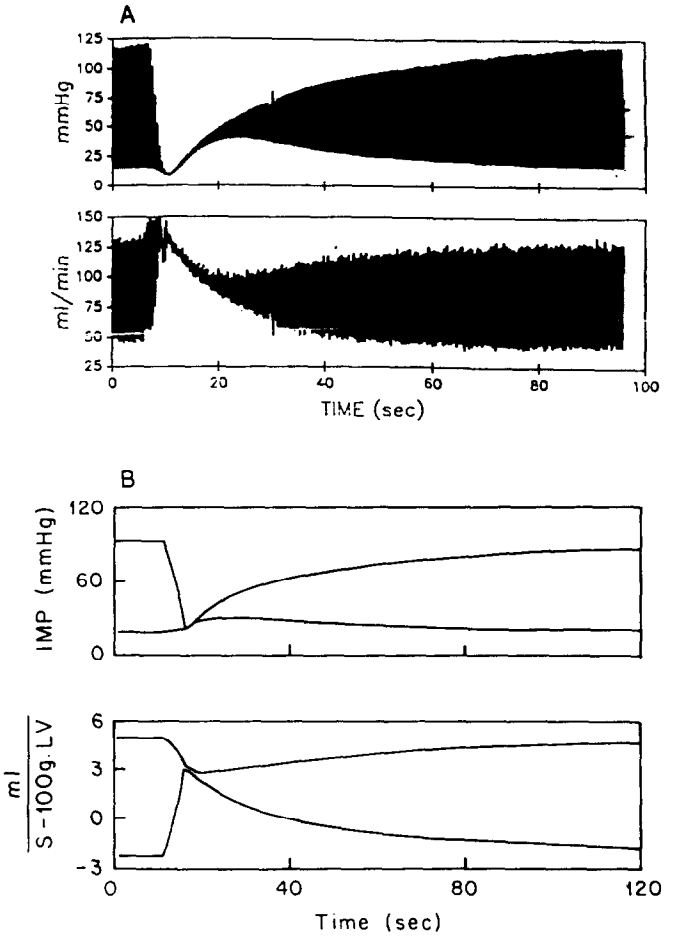

FIG. 15. *IMP* and coronary flow in the transient arrest of an empty heart. (A) Experimental data of Kresh [2] (reproduced from ref. [2], with permission). (B) Model simulation.

DISCUSSION

The integrated model.

The major importance of the integrated LV model is that it allows us to address the following aspects of the cardiac system.

(1) The interstitial fluid mass balance within the LV wall. Previous flow-mechanical models [5, 6] do not account for this fluid balance and therefore cannot evaluate the myocardial interstitial fluid content at different loading and contractile conditions.

(2) Effects of the circulation on the LV mechanics.

Table 2. Effect of perfusion pressure on end-diastolic LV compliance

P_{ao} (mmHg)	$C_{ED} = \frac{dV_{ED}}{dP_{ED}}\left(\frac{ml}{mmHg}\right)$
60	1.62
100	1.25
150	0.89

The coronary flow affects the LV mechanics through: (1) the vascular volume and (2) fluid flow across the capillary wall. The interstitial fluid mass balance provides an additional linkage between the myocardial blood flow and mechanics to describe the LV performance. These effects could not be accounted for in previous models.

(3) Wall compressibility. The generally used LV wall incompressibility condition, is substituted here by equation (5), which provides the LV wall volume in terms of its components. This approach allows us to evaluate the components of the wall volume, and their dynamics, at the prevailing conditions. The LV performance is thus uniquely determined, allowing us to calculate different steady state (e.g. arrested and beating hearts) and transient conditions and study the effects of blood volume changes during the heart beat. Furthermore, it enables us to study the complex effects of pathologies associated with disturbances in the fluid transport, such as edema, on myocardial mechanics and coronary flow.

(4) The LV global performance (mechanical, blood flow and fluid and mass transport) is directly related

to the myocardial contractile activity, the myocardial structure and the boundary and loading constrains. Thus, the LV variables are related directly to the myocardial activity and not to dependent variables, such as the *IMP* or the *LVP*, which are passive results of the muscle activity. This relation will be of major relevance in investigating the effect of the myocardial metabolic supply, through the circulation, on the LV performance.

Diastolic IMP and interstitial fluid content. Fluid transport, in combination with the mechanics and the coronary flow, has a major effect in determining the level of the diastolic *IMP*. This effect is demonstrated experimentally [2] (Fig. 15(A)), during the period of total and partial myocardial arrest, where the decrease in the mean *IMP* following the pentobarbital infusion allows for the transport of fluid into the interstitial space and causes the elevation of the diastolic *IMP* from the beating heart value towards the arrested heart value. The experiment demonstrates that as the heart is arrested, the *IMP* initially equals the same diastolic *IMP* as in the beating heart which corresponds to the fluid content and total wall volume at that moment. Then, as the transcapillary fluid flux increases and the lymphatic flow decreases due to the reduction of the *IMP*, the interstitial volume starts to increase and the *IMP* starts to increase from the end diastolic beating heart value to the arrested heart value while the muscle is still almost totally arrested (see also Fig. 6(B)). As the myocardium slowly starts beating again, the diastolic *IMP* value decreases and the peak systolic value increases back to their values in the normal beating conditions. This is due to the overall increase in the *IMP* which increases the lymphatic outflow and lowers the transcapillary fluid flux, thus decreasing the interstitial fluid content, and affects the blood content too. The corresponding flow transients follow the trends of the *IMP* dynamics. The flow immediately after arrest remains close to its diastolic value and then decreases to the arrested heart value as the *IMP* increases. As the muscle activity resumes the flow and *IMP* return to their beating heart values.

Evidently, changes in the diastolic *IMP* value may modify the initial sarcomere length and hence affect the systolic stresses and *IMP*. This is observed in Fig. 6(B) where an increase in coronary perfusion pressure causes an increase in diastolic *IMP* and a corresponding increase in the systolic *IMP*.

Autoregulation. Coronary autoregulation is not accounted for in the present model. However, it has been suggested that an increase in *IMP* due to an increase the in perfusion pressure may affect the circulation by externally compressing the blood vessels. Although this postulated 'Tissue Pressure' [33] mechanical autoregulatory mechanism may contribute to the overall response of the coronary flow to perfusion pressure, it does not provide a viable explanation of the flow autoregulatory phenomena. The results shown here indicate that the flow rate increases as the perfusion pressure is elevated even though the *IMP* increases, suggesting that flow autoregulation is not a purely mechanical phenomena.

Coronary flow oscillations. The combined effects of myocardial mechanics, blood flow and fluid transport are also manifested in the oscillatory flow amplitude (*OFA*). For example, variations in the *OFA* as a function of the perfusion pressure can be explained in terms of two related factors: (1) the dependence of the resistance and capacitance values on the local vessel transmural pressure and (2) the variations in the *IMP* due to changes in circulatory conditions and a shift of fluids into the extravascular space.

Coronary elastance. Krams *et al.* [27, 28] have explained the effects of contractility, coronary perfusion pressure and LV pressure on the *OFA* in terms of an elastance concept, i.e. the resistances and capacitances of the myocardial-coronary system are time varying and may be represented by a time dependent coronary elastance, *CE(t)*. According to Kresh [2], Krams *et al.*'s [28] coronary elastance is similar to the intramyocardial pump concept. When applied to the coronary flow the integrated model is, in fact, Krams *et al.*'s [27, 28] elastance or the intramyocardial pump concepts expressed in a structural and quantitative form. Thus, rather than being phenomenologically described by a time dependent 'coronary elastance' or an intramyocardial pump, the coronary flow here is directly related to the myocardial structure and activity.

Contractility. Myocardial contractility is the principal factor in determining the global LV performance. This is clearly reflected by the major changes in myocardial mechanics, coronary flow and fluid and mass transport that follow changes in the muscle contractility condition as shown in Kresh's experiment [2].

The effect of myocardial contractility on the coronary flow dynamics is manifested by an increase of the *OFA* with increasing contractility (Fig. 8). The effect of muscle contractility on flow dynamics is demonstrated in Kresh's transient contractile dysfunction experiment [2]. A reduction in muscle force reduced the systolic *IMP* and thus caused a transient decrease in coronary flow oscillations. Fluid accumulation in the myocardium due to the reduced mean *IMP* causes an increase in diastolic *IMP* and a concomitant decrease in mean coronary flow. The experimental results [2] and accompanying simulation emphasize the fact that the LV performance, expressed in terms of LV pressures (zero in this case) and volumes, *IMP* and fluid shift dynamics as well as coronary flow dynamics, are derived from the primary active force development in the sarcomere.

Myocardial edema. The variations in the flow and mechanical variables during myocardial edema simulated here by a reduction of the lymphatic outflow is another feature which demonstrates the importance of including fluid transport effects in an integrated LV model. Shifts in the myocardial fluid balance associ-

ated with the development in edema may exist in numerous pathological and experimental conditions; these may be due to abnormal lymphatic drainage, abnormal capillary permeability or abnormalities in the contractile function. Further theoretical experimental studies are needed to clarify the importance of the different pathophysiological mechanisms affecting the fluid balance and their relative importance.

Limitations. The study is obviously limited by the various simplifying assumptions used in the proposed model. Obviously, this approach neglects transmural heterogeneities. Yet it can still yield important insights based on the wall-averaged complex interactions between mechanics, blood flow and across capillary transport. Future studies with an integrated model involving transmural distribution across the wall should yield further insight.

A more realistic wall geometry will obviously lead to a more accurate simulation of reality. However, the additional complexity of a realistic geometry of the LV is presently unwarranted.

Myocardial transport phenomena are limited here to water and albumin. Other macromolecules are obviously involved in the osmotic processes and should eventually be studied. Transport phenomena related to the metabolic processes associated with energy consumption and the flow autoregulatory mechanisms should also be considered in future studies.

CONCLUSIONS

The model integrates myocardial mechanics, coronary flow and intramyocardial fluid and mass transport. The main strength of the model used lies in its ability to decipher some of the complex interactions between myocardial mechanics, coronary flow and fluid and mass transport and to predict the effect of coronary perfusion pressure on the myocardial mechanical conditions and the interstitial fluid accumulation under various experimental and pathophysiological conditions. The effect of perfusion pressure on LV compliance is also predicted. The analysis of the arrested and the beating hearts under isovolumic and zero isobaric conditions, transient changes in myocardial force and the simulation of edema attest to the importance of adding fluid and mass transport considerations into LV modeling and of assuming a LV integrated approach.

Acknowledgements—This study was made possible by a Post Doctoral grant from the Lady Davis Foundation (D.Z.). The study was also supported in part by a Technion grant for the promotion of research at the Technion (S.S.) and the Joseph and Edythe Jackier Endowment Fund, Detroit, U.S.A. The continuous support of the Michael and Adelaid Kennedy Leigh Fund, London, U.K. is also acknowledged with great appreciation.

REFERENCES

1. G. A. Laine and H. J. Granger, Microvascular, interstitial and lymphatic interactions in normal heart, *Am. J. Physiol.* **249,** H834–H842 (1985).
2. J. Y. Kresh, Myocardial modulation of coronary circulation (letter), *Am. J. Physiol.* **257,** H1934–H1935 (1989).
3. A. Fukui, S. Yamaguchi, Y. Tamada, H. Miyawaki, G. Baniya and M. Shirakabe, Different effects of coronary perfusion pressure on diastolic properties of left and right ventricles, *Circulation* **84,** II-45 (1991).
4. A. D. McCulloch, P. J. Hunter and B. H. Smaill, Mechanical effects of coronary perfusion in the passive canine left ventricle, *Am. J. Physiol.* **262,** H523–H530 (1992).
5. T. Arts and R. S. Reneman, Interaction between intramyocardial pressure (*IMP*) and myocardial circulation, *J. Biomed. Engng* **107,** 51–56 (1985).
6. R. Beyar and S. Sideman, Time dependent coronary blood flow distribution in the left ventricular wall, *Am. J. Physiol.* **252,** H417–H433 (1987).
7. R. S. Chadwick, A. Tedgui, J. B. Michel, J. Ohayon and B. I. Levy, Phasic regional myocardial inflow and outflow: comparison of theory and experiments, *Am. J. Physiol.* **258,** H1687–H1698 (1990).
8. D. D. Streeter, H. M. Spotnitz, D. P. Patel, J. Ross and E. H. Sonnenblick, Fiber orientation in the canine left ventricle during diastole and systole, *Circ. Res.* **24,** 339–347 (1969).
9. J. Ohayon and R. S. Chadwick, Effects of collagen microstructure in the mechanics of the left ventricle, *Biophys. J.* **54,** 1077–1088 (1988).
10. T. Arts, P. C. Veenstra and R. S. Reneman, Transmural course of stress and sarcomere length in the left ventricle under normal hemodynamic circumstances. In *Cardiac Dynamics* (Edited by J. Baan, A. C. Arntsenius and E. L. Yellin), pp. 115–122. Martinus Nijhoff, The Hague (1980).
11. R. Beyar and S. A. Sideman, Computer study of the left ventricular performance based on fiber structure, sarcomere dynamics and transmural electrical propagation velocity, *Circ. Res.* **55,** 358–375 (1984).
12. R. S. Chadwick, Mechanics of the left ventricle, *Biophys. J.* **39,** 279–288 (1980).
13. E. Nevo and Y. Lanir, Structural finite deformation model of the left ventricle during diastole and systole, *Trans. ASME* **111,** 342–349 (1989).
14. F. Gonzalez and J. B. Bassingthwaighte, Heterogeneities in regional volumes of distribution and flows in rabbit heart, *Am. J. Physiol.* **258,** H1012–H1024 (1990).
15. J. A. E. Spaan, Coronary diastolic pressure-flow relation and zero flow pressure explained on the basis of intramyocardial compliance, *Circ. Res.* **56,** 293–309 (1985).
16. R. Beyar, R. Camminker, D. Manor and S. Sideman, Coronary flow patterns in normal and ischemic hearts: Transmyocardial and artery to vein distribution, *Ann. Biomed. Engng* **21,** 1–24 (1993).
17. J. Y. Kresh, M. Fox, S. K. Brockman and A. Noordergraaf, Model-based analysis of transmural vessel impedance and myocardial circulation dynamics, *Am. J. Physiol.* **258,** H262–H276 (1990).
18. O. Kedem and A. Katchalsky, Thermodynamic analysis of the permeability of biological membranes to non-electrolytes, *Biochim. Biophys. Acta* **27,** 229–246 (1958).
19. J. G. Pinto, A constitutive description of contracting papillary muscle and its implications to the dynamics of the intact heart, *ASME J. Biomed. Engng* **109,** 181–190 (1987).
20. G. H. Pollack and J. W. Krueger, Myocardial sarcomere mechanics: some parallels with skeletal muscle. In *Cardiovascular System Dynamics* (Edited by Y. Baan, A. Noordegraaf and J. Raines), pp. 3–10. MIT Press, Cambridge, MA (1978).
21. T. S. Feit, Diastolic pressure volume relationship and distribution of pressure and fiber extension across the wall of a model left ventricle, *Biophys. J.* **28,** 143–166 (1979).
22. E. Braunwald, J. R. Ross and E. H. Sonnenblick (Edi-

tors), *Mechanism of Contraction of Normal and Failing Heart* (2nd Edn). Little, Brown and Co., Boston (1976).
23. P. Sipkema and N. Westerhof, Mechanics of a thin walled collapsible microtube, *Ann. Biomed. Engng* **109,** 181–190 (1987).
24. W. M. Chilian, S. M. Layne, E. C. Klausner, C. L. Eastham and M. L. Marcus, Redistribution of coronary microvascular resistance produced by dipyridamole, *Am. J. Physiol.* **256,** H383–H390 (1989).
25. J. C. Parker, M. A. Perry and A. E. Taylor, Permeability of the microvascular barrier. In *Edema* (Edited by N. C. Staub and A. E. Taylor), pp. 160–167. Raven Press, New York (1984).
26. D. Zinemanas, R. Beyar and S. Sideman, Intramyocardial fluid transport effects on coronary flow and LV mechanics. In *Interactive Phenomena in the Cardiac System* (Edited by S. Sideman and R. Beyar), pp. 219–231. Plenum Press, New York (1993).
27. R. Krams, P. Sipkema and N. Westerhof, Coronary oscillatory flow amplitude is more affected by perfusion pressure than ventricular pressure, *Am. J. Physiol.* **258,** H1889–H1898 (1990).
28. R. Krams, P. Sipkema, J. Zegers and N. Westerhof, Contractility is the main determinant of coronary systolic flow impediment, *Am. J. Physiol.* **257,** H1936–H1944 (1989).
29. J. Y. Kresh, F. Frash, M. McVey, S. K. Brockman and A. Noordergraaf, Mechanical coupling of the myocardium with coronary circulation in the beating and arrested heart, *Circulation* **84,** II-45 (1990).
30. J. B. Bassingthwaigthe and C. A. Goresky, Modeling in the analysis of solute and water exchange in the microvasculature. In *Handbook of Physiology* (Edited by E. M. Renking and C. C. Michel), pp. 549–626. American Physiological Society, Bethesda, U.S.A. (1984).
31. R. J. Baird, M. M. Goldbach and A. Rocha, Intramyocardial pressure the persistence of its transmural gradient in the empty heart and its relationship to myocardial oxygen consumption, *J. Thor. Card. Surg.* **64,** 635–646 (1972).
32. F. L. Abel, R. R. Zhao and R. F. Bond, Contribution of extravascular compression to reduction of uniaxial coronary blood flow, *Am. J. Physiol.* **262,** H68–H77 (1992).
33. J. I. E. Hoffman and A. E. Spaan, Pressure-flow relations in coronary circulation, *Physiol. Rev.* **70,** 331–390 (1990).